Instruments and Methods

A ground-based radar for measuring vertical strain rates and time-varying basal melt rates in ice sheets and shelves

Keith W. NICHOLLS,[1] Hugh F.J. CORR,[1] Craig L. STEWART,[2] Lai Bun LOK,[3]
Paul V. BRENNAN,[3] David G. VAUGHAN[1]

[1]British Antarctic Survey, Natural Environment Research Council, Cambridge, UK
[2]Scott Polar Research Institute, University of Cambridge, Cambridge, UK
[3]Department of Electronic & Electrical Engineering, University College London, London, UK
Correspondence: Keith W. Nicholls <kwni@bas.ac.uk>

ABSTRACT. The ApRES (autonomous phase-sensitive radio-echo sounder) instrument is a robust, lightweight and relatively inexpensive radar that has been designed to allow long-term, unattended monitoring of ice-shelf and ice-sheet thinning. We describe the instrument and demonstrate its capabilities and limitations by presenting results from three trial campaigns conducted in different Antarctic settings. Two campaigns were ice sheet-based – Pine Island Glacier and Dome C – and one was conducted on the Ross Ice Shelf. The ice-shelf site demonstrates the ability of the instrument to collect a time series of basal melt rates; the two grounded ice applications show the potential to recover profiles of vertical strain rate and also demonstrate some of the limitations of the present system.

KEYWORDS: Antarctic glaciology, glaciological instruments and methods, ice shelves, ice/ocean interactions, radio-echo sounding

INTRODUCTION

Over the past decade there has been a growing interest in the response of ice-shelf basal melt rates to changes in the underlying ocean. This has resulted from the recognition that the flow of ice streams and the inland ice sheets they drain is sensitive to changes in the geometry of downstream ice shelves (e.g. Shepherd and others, 2004; Schoof, 2007). The study of ice-shelf–ocean interactions has been hindered, however, by a lack of data from the ocean cavity beneath the ice shelves.

The need for basal melt rates from ice shelves

Deploying oceanographic instruments through hot-water drilled access holes has formed the mainstay of efforts to acquire time series of ocean observations from sub-ice-shelf cavities. However, the logistical cost of this approach has ensured that such time series are few in number: the cavity beneath the Filchner–Ronne Ice Shelf, Antarctica, is one of the most explored using this technique (Nicholls and others, 2009), yet it has yielded fewer than a dozen moored time series scattered over the past 25 years.

In recent years, there have been a small number of excursions beneath ice shelves by autonomous vehicles, such as Autosub2 (Nicholls and others, 2006, 2008) and Autosub3 (Jenkins and others, 2010). Although these vehicles give a unique view of the topography of the ice base and the sea floor, they are presently limited to providing summer snapshots of the oceanographic conditions within the cavities. The vehicles are also expensive to manufacture, and require a ship to get to within range of the ice front.

The difficulty in obtaining measurements from beneath ice shelves has led to a high degree of reliance on numerical models to provide a 'view' of the oceanographic conditions within the cavity (e.g. Williams and others, 1998). Ocean models rely on parameterizations to represent processes that

the coarseness of their discretization prevents them from resolving. Data from the cavities are therefore needed to develop and refine the parameterizations, and to validate the simulations. In the future, data from cavities might also be valuable for helping control models using data assimilation techniques.

Although direct measurements of the oceanographic conditions are difficult and costly, the effect of those conditions on the ice – the exchange of mass at the ice base – is more readily observable. The basal melt rate of ice shelves has been of glaciological interest, as it represents a major component of the overall ice-shelf mass budget. From an oceanographic perspective, measurements of basal melt rate are direct measurements of buoyancy flux into the ocean at the ice base, and also give an indication of the heat flux from the ocean. Melt rates clearly depend on the ocean properties within the cavity, and the ocean circulation that carries heat and salt around the system. This means that basal melt rates are an excellent diagnostic for the performance of models in predicting both the water's circulation within a sub-ice-shelf cavity, and its interaction with the overlying ice.

The basal mass balance of an ice shelf has in the past been determined by glaciological studies that require the assumption that the ice shelf is in steady state. The basal mass balance was computed using repeat surveys of strain networks, surface accumulation measurements, and knowledge of the local ice velocity and thickness gradients (e.g. Bishop and Walton, 1981; Jenkins and Doake, 1991). Satellite techniques have also been employed. These use the same principle, but ice thickness gradients are obtained from inversion of surface elevation by using the assumption that the ice shelf is in hydrostatic equilibrium (e.g. Vaughan and others, 1995; Fricker and others, 2000), and velocity and strain data are obtained either from feature tracking or from satellite synthetic aperture radar interferometry (e.g. Rignot

and others, 2013). The steady-state assumption has started to be addressed by using repeat altimetry to determine the temporal rate of change of ice thickness (Pritchard and others, 2009; Dutrieux and others, 2013; Moholdt and others, 2014).

A distinct advantage of the satellite method is that it yields excellent spatial coverage. There are several disadvantages, however. As in the case of the traditional ground-based method, the calculated melt rates are long-term averages (typically a year or more), and rely on the assumption that the vertical strain rate in the ice is constant with depth, an assumption known to fail in the vicinity of grounding lines (Jenkins and others, 2006). The satellite-based datasets require substantial spatial averaging to reduce noise. Furthermore, the correction required to remove the steady-state assumption is very sensitive to assumptions about compaction rates in the upper firn.

Phase-sensitive radar

Ground-based phase-sensitive radar with glaciological application has its roots in the pioneering work during the 1970s by researchers at the University of Bristol (e.g. Walford and Harper, 1981). But with emphasis turning to sophisticated airborne systems, for some decades ground-based radar developed only slowly. However, since the turn of the century, the use of ground-based phase-sensitive radar (pRES) to measure both ice-shelf basal melt rates (Corr and others, 2002; Jenkins and others, 2006; Dutrieux and others, 2014) and vertical strain rates in ice sheets more generally (Kingslake and others, 2014) has been increasing. The equipment used is described by Corr and others (2002) and is based on a vector network analyser configured as a step-frequency radar. By considering the ice sheet as the 'device under test' its complex scattering characteristics can be measured over a broad range of frequencies, with an inverse Fourier transform used to recover the equivalent impulse response. The phase of the response is retained, and serves to improve the precision of the measurement: a signal-to-noise ratio of 17 dB allows a 1° change in phase to be detectable, corresponding to a 1 mm change in range in the case of a system centred on 300 MHz. Ground-based phase-sensitive radar has been able to track the relative vertical motion of internal layers within the ice as well as the ice base. In this way, it is possible to account for the various factors affecting the range between antennas and ice base – snow accumulation between visits, snow densification and ice strain – allowing the calculation of the basal melt rate at a point in any location that has identifiable internal layers, including near grounding lines.

The advantages of pRES are that no assumption of steady state is required (as it is a Lagrangian measurement); the vertical profile of ice strain can be determined, removing the assumption that it is constant with depth; the footprint of the measurement is small; and the measurement is very precise. The disadvantages are that the equipment is heavy and expensive, requiring a portable generator to keep the instrument running and at room temperature, and the limited spatial scale of the footprint makes it difficult to obtain a spatially averaged melt rate over regions of strong basal topography. A key disadvantage of pRES, and one that is shared by satellite techniques, is that the measurements are averages over the interval between revisits, typically a few days during the summer or a complete year or more. This is one of the disadvantages that the instrument described here was designed to overcome.

pRES on grounded ice sheets

The ability to measure vertical strain rates and the compaction rate in the firn layer has made the pRES technique attractive to researchers studying the glaciology of grounded ice sheets, for whom these are key quantities. A particular use has been in the study of ice divides where knowledge of vertical strain rates can help disentangle past patterns of accumulation and ice flow (Gillet-Chaulet and others, 2011; Kingslake and others, 2014).

A related application is in helping to create an ice sheet's age–depth relationship, a prerequisite for the interpretation of the climatic record locked within an ice core. A number of different techniques are currently used to establish the date and the location at which a given particle within the ice core was deposited, including counting annual layers, identifying dated volcanic horizons and comparing patterns of chemical species with those from other ice cores. Where direct chronological information is either unavailable or incomplete, a flow model, constrained by the existing observables, can be applied to give a complete age–depth function. A particularly valuable constraint is the profile of vertical strain rate, which can be obtained using the pRES technique (Martin and others, 2015).

Measurement of time-varying vertical velocities

Timescales of variability of vertical strain rates in grounded ice are long, and we would expect there to be no useful information about short-term variations that would be lost by revisiting sites annually and obtaining annual average values. Basal melt rates of ice shelves, however, are subject to variability on the timescales of ocean variability, from interannual down to tidal and below, and there are several reasons why measuring the time variability of ice-shelf melt rates might benefit the ice-shelf–ocean community:

1. Seasonally and interannually varying forcing from the ocean will in some cases serve as a useful proxy for longer-term climate variability. The ability to observe the way the intensity of basal melt rates is affected by a changing forcing will give clues as to how the ice-shelf–ocean system will respond to future changes in climate.

2. Melt rate time series from carefully chosen sites on ice shelves will provide a source of stringent validation data for numerical models being used to predict ice-shelf–ocean interactions. Alternatively, such datasets could be used to help control models using assimilation techniques.

3. When melt rate time series are available at sites where contemporaneous sub-ice-shelf oceanographic data are also available from the oceanic boundary layer adjacent to the ice base, details of the vertical mixing processes can be elicited and parameterizations that are used in numerical models can be tested.

Here we describe an instrument that has been developed as a field-capable replacement for pRES. It has been designed to be deployed for long periods, making several measurements each day, to yield not only a long-term average of basal melting, but also a time series capable of showing variation in melt rate on timescales from tidal to seasonal and longer. The technical aspects of the radar have been described in detail elsewhere (Brennan and others, 2013). The aim of this contribution is to report experiences of its use and to discuss the utility of the instrument from a user's

point of view. We first give a brief description of the new radar's theory of operation and its essential specifications, and then present a set of case studies, one showing the results from a month-long deployment of the system on an ice shelf, and two others from more demanding, non-ice-shelf environments.

INSTRUMENT DESCRIPTION

Radar

The design and technical details for the instrument's radar board are described by Brennan and others (2013). Here we briefly summarize the theory of operation of the instrument and how it is used as a field-deployable system.

The radar uses the frequency-modulated continuous wave (FMCW) technique, in which a tone sweeps from 200 to 400 MHz over a period of 1 s to form a chirp. The output power to the transmit antenna is nominally 100 mW. After amplification, the received signal is mixed with a replica of the transmitted to yield a de-ramped signal comprising frequencies that depend on the delay between the transmitted and received chirps. For a reflection from the bed of a 2.1 km deep ice sheet, the frequency of the de-ramped signal is ~5 kHz. The de-ramped signal is then passed to an active filter that preferentially amplifies the higher frequencies, thus allowing convenient enhancement of weaker signals from more distant reflectors to compensate for geometric spreading and dielectric absorption. The amplified output is digitized and the data stored on memory cards (SD, or Secure Digital cards). In order to maintain phase-coherency, the time at which the samples are converted by the analogue-to-digital converter (ADC) is precisely and consistently aligned with the start of each transmitted chirp.

There are two principal subsystems in our implementation of the instrument: the radar board and the radar controller, which also logs the data. The low power consumption and tolerance to cold of both radar board and controller are the key attributes that make the radar a field-capable instrument. The radar can be operated either in an attended or unattended mode, and has been designated autonomous-pRES or auto-pRES (ApRES). When attended, the controller communicates with the user via an Ethernet interface to a computer running a web browser. This enables the user to operate the instrument in a survey mode, downloading data after each measurement. In unattended mode, the computer is disconnected and the instrument runs according to parameters in a configuration file on the SD card. Those configuration data determine how often measurements are to be made, how many chirps are to be collected for each measurement, the levels of amplification to be used in the receiver, and many other details of the instrument's operation.

Various aspects of the design contribute to making the instrument suited to being used in unattended mode. The instrument runs on a 6–16 V source, with a maximum current draw at 6 V of ~1 A, which reduces to ~200 μA during sleep between measurements. A typical measurement will last for 1–2 min, coherently stacking 20–100 consecutive chirps, so that 100 Ah of battery capacity would power 10–20 measurements each day for a period of a year. The components used in the instrument are specified to a minimum temperature of –40°C. An Iridium data link is built into the controller, and also a GPS receiver, primarily to help with the precise
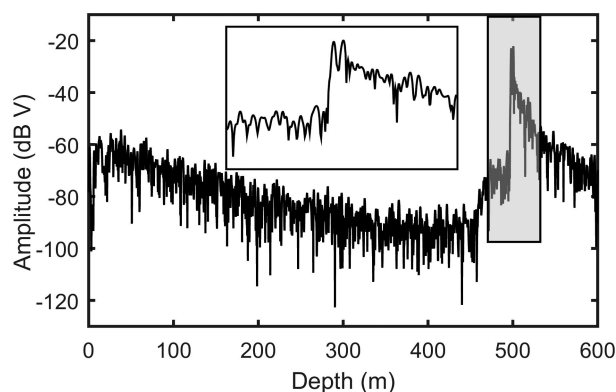

Fig. 1. ApRES return from Pine Island Glacier Ice Shelf, with inset enlargement showing the nature of the double return from the base.

timing of observations. The GPS fix is included in the transmission via the Iridium link, helping in the recovery of an instrument deployed on a moving ice sheet. The Iridium link is two-way, allowing remote reconfiguration of most aspects of the radar's operation. The instrument is housed in a waterproof plastic case with dimensions 410 mm × 320 mm × 170 mm, and weight 4.2 kg.

Imaging capability

A monostatic radar system uses a co-located or pseudo-co-located receive (Rx) and transmit (Tx) antenna pair. In our case, a transmit antenna is typically located ~5 m from the receive antenna. As the FMCW technique relies on transmitting and receiving simultaneously, the minimum distance between the antennas is determined by the acceptable level of direct breakthrough between them, which in turn is determined by the input compression point of the radar's receiver circuitry. For targets more distant than a few antenna separations, the received signal can be regarded as coming from a radar with antennas collocated at a point midway between the phase centres of the two actual antennas. This raises the possibility of an arrangement of multiple (N_r) receive and multiple (N_t) transmit antennas, where the midway points of all $N_r \times N_t$ combinations form an array of virtual pairs, or, in effect, a synthetic aperture.

ApRES has the capability of switching between up to eight transmit and eight receive antennas to provide the possibility of imaging (yielding 64 virtual antenna pairs). This is of value in cases where the basal reflector gives a complicated return. An example from Pine Island Glacier, Antarctica, is shown in Figure 1. (In this and all similar figures the range of returns is calculated assuming a constant ice permittivity of 3.18.) Here there are two separate returns at a range that is consistent with the approximate ice thickness. Subsequent visits showed that the range to different returns changed at different rates, making an assessment of the basal melt rate difficult. An imaging capability offers the opportunity to resolve the ambiguity in such data, giving an effective angular resolution of 5–10°, depending on the details of the antenna distribution. The imaging aspect of the instrument will be discussed in a manuscript in preparation.

Antennas

When operated in attended mode the instrument is generally used at many sites in a single field study. The antennas therefore need to be robust enough to withstand the rigours

Fig. 2. (a) Photograph of a deployment on the Ronne Ice Shelf, Antarctica. The ApRES is in the yellow case visible in the background, between the two antennas, and shown enlarged in the inset. (b) Photograph shows one constructed bow-tie antenna (left) and another being assembled. The bow tie comprises copper triangles connected to a balun and fixed to a polycarbonate roofing sheet with adhesive tape. An aluminium reflector is then supported by crossed dividers before the lid is taped closed.

of field use. They also need to be reasonably compact, lightweight and able to operate over a broad bandwidth (200–400 MHz). To suit these requirements, a demountable skeleton slot antenna has been developed (Fig. 2a). When packed for shipping, a pair of the antennas fits into a box 0.72 m × 0.72 m × 0.1 m in size, and weighs 12 kg.

Antennas for instruments that are to be deployed in one location for extended periods have different design requirements. In particular it is important that the properties of the antennas do not change significantly during the deployment. An open-structure antenna such as the skeleton slot devices shown in Figure 2a needs to be protected from filling with snow; a change in the dielectric properties of the spaces within the antenna structure would significantly alter its properties during the time series. In addition, the skeleton slot antennas are relatively expensive, and such a robust solution is not required if they are not going to be routinely moved from place to place.

A cavity-backed bow-tie antenna was developed to provide a cost-effective solution suitable for long-term deployment; it is housed in a corrugated plastic box, yielding a lightweight, flat-pack solution, at less than one-tenth the cost of the skeleton slot antenna, and which can be buried just below the snow surface (Fig. 2b). The bow-tie dimensions were calculated such that the antenna gives the required input impedance when buried in snow. Having a flat-pack solution is particularly important for deploying several sites, as the volume of the assembled antenna boxes would quickly become unfeasibly large.

RESULTS FROM TRIAL SITES

The ApRES instrument has now been tested at several locations, both on grounded ice and on ice shelves. The aim on grounded ice is to investigate the vertical profile of ice velocity, i.e. the variation in vertical strain rate with depth.

On ice shelves with no significant topography on spatial scales of the ice thickness, and far from grounding lines, the vertical strain rate is constant with depth, and the objective is more often to measure the basal melt rate. In the vicinity of grounding lines, where tidal bending is significant, phase-coherent radar (pRES) has been used to study vertical strain rates, yielding direct measurements of elastic properties of the ice column (Jenkins and others, 2006).

Here we present trial data from three sites that highlight the strengths and have exposed the limitations of the present ApRES. The first example is from an ice-shelf site where the primary goal was to obtain a time series of basal melt rates. The other two sites were on grounded ice: Pine Island Glacier, where the aim was to determine vertical strain rates in the ice column; and over the deep ice at Dome C, where the aim was to examine the limits of the instrument's ability to measure the relative motion of internal layers.

Ross Ice Shelf

During the 2010/11 field season the ANDRILL project used a hot-water drill to create an access hole through the Ross Ice Shelf at Coulman High (Arzeno and others, 2014) (Fig. 3). The hole gave access to the water column beneath the ice shelf for oceanographic profiling measurements and for the installation of permanently moored instruments for long-term measurements. As part of the study into interactions between the Ross Ice Shelf and the ocean, an ApRES instrument was used both in survey (attended) mode and also in unattended mode. Figure 3 shows the locations of the network of sites visited during a 10 day, snowmobile-based survey.

Here we present results from an example site established during the 2012/13 field season and reoccupied in 2013/14. The results illustrate the nature of the dataset obtained from the radar, and how internal layer motion can be used to separate three processes, in addition to basal melting, that
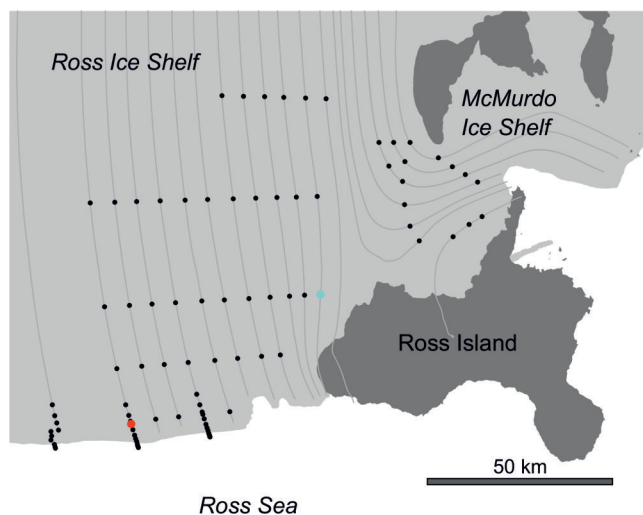
Fig. 3. Map of Ross and McMurdo ice shelf study area. Grey lines are ice flow lines; black dots are repeat ApRES stations; cyan dot is repeat ApRES station with data shown in Figure 4; red dot shows location of Coulman High, a time series from which is shown in Figure 5.

affect the range of the ice base from the antenna: first, the changing vertical position of the antennas (accumulation of snow between visits); second, compaction effects in the snow–firn–ice column; and third, vertical strain in the ice resulting from horizontal ice divergence.

On each visit the instrument stacked 100 chirps over a period of ~3 min, to give 100, 1 s long, time series. The chirps were averaged, and an averaged chirp from one of the visits is shown in Figure 4a. The strength of the principal tone related to the first basal reflection is clear in Figure 4a (inset), although the many other frequency components that result from reflections from targets at different ranges can only be discerned by carrying out a spectral analysis. The 1 s-long average time series was doubled in length by zero-padding, and then a Blackman window was applied (Brennan and others, 2013). Figure 4b shows the Fourier transform of the padded, windowed versions of the signals from the two visits, after alignment by cross-correlating the amplitudes of internal reflections immediately below the firn layer. Alignment accounts for changes in antenna position that result from snow accumulation, the first of the three processes discussed above. Figure 4b illustrates the exceptionally strong basal return obtained at this site. Second and third return multiples are present (not shown), resulting from re-reflection from the snow surface.

By comparing the phase of individual internal reflectors their relative motion was calculated (Fig. 4c). As the two records have already been aligned at a depth below the firn (at ~80 m depth), the datum for the relative motion was at around that depth. The phase shift between the two records increases with depth, and has to be carefully tracked to avoid wrap errors as the signal strength weakens and the phase becomes less well defined. The effects of compaction in the upper 70 m and the linearly increasing offsets with
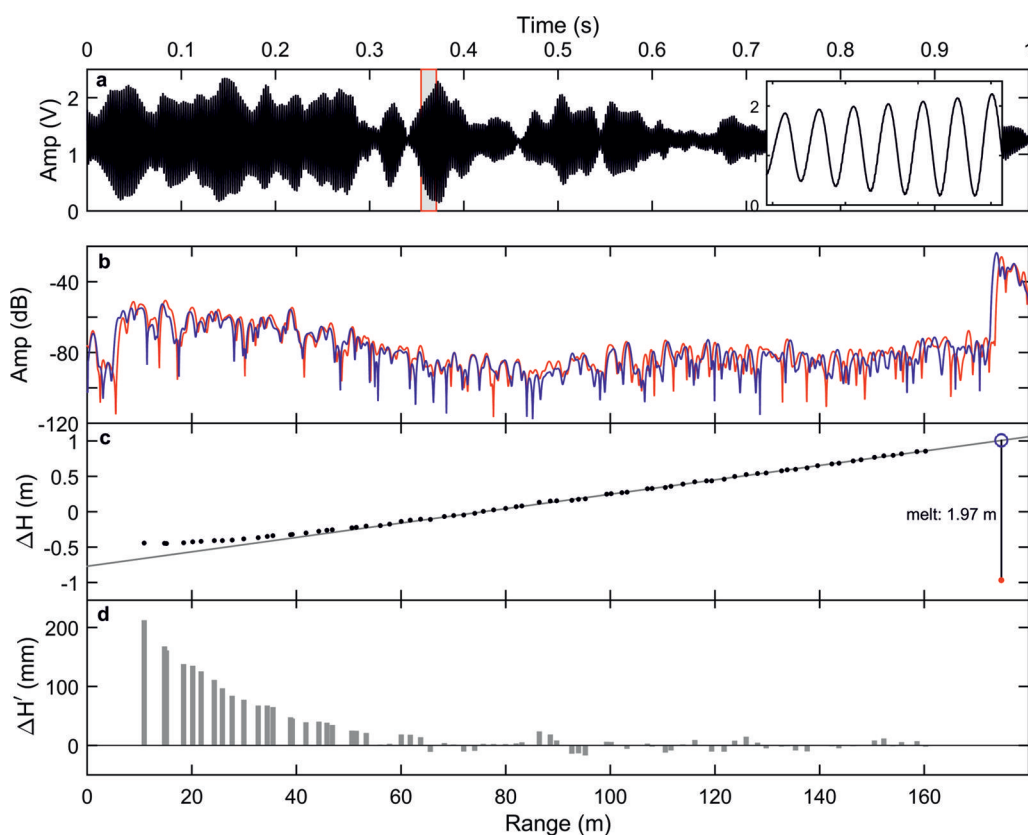

Fig. 4. Results from two visits to one sample site (location marked by cyan dot in Fig. 3). (a) Raw time series showing averaged chirp. Inset illustrates dominant tone, associated with basal return. (b) Fourier transform of mean chirps from first (red) and second (blue) visits after aligning to account for snow accumulation. (c) Relative internal layer motion (black dots), linear fit between 70 m and 160 m (grey line), basal echo offset due to melt (red dot). (d) Compaction extracted as deviation from the straight line fit in (c). Here we assume the velocity of radio waves to be constant with depth. For a quantitative study of compaction, the analysis would need to account for the dependence of the velocity of radio waves on the changing air content.
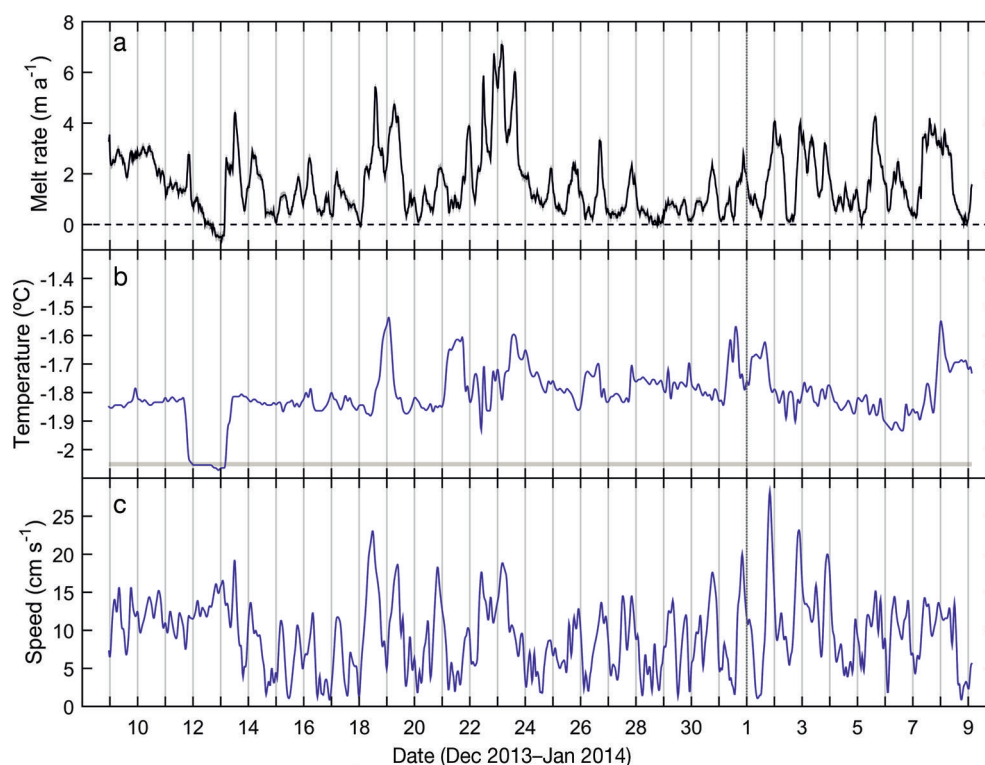
Fig. 5. (a) Observed basal melt rate. (b) Water temperature 14 m below the ice base. The in situ freezing point is indicated by the dashed line. (c) Water speed 14 m below the ice base.

depth due to vertical strain (resulting at this site from ice convergence) are clearly visible. The firn compaction signal, extracted by removing an assumed linear vertical strain signal from the record, is shown in Figure 4d. In the case of the basal return, the difference in range between the two records is likely to be equivalent to many wavelengths, so the measured phase difference must be added to the change in range found by the shift in the amplitude peak. The displacement of the basal return from the straight line associated with a constant vertical strain rate within the ice column results from the vertical motion associated with basal melting, in this case 1.97 m (Fig. 4c).

The instrument was also deployed unattended for various extended periods at the drill site itself (Fig. 3, red dot). Here we focus on one 30 day long time series of data acquired at the drill site in December 2013. The instrument was configured to record 10 chirps every 30 min, with each set taking about 20 s to acquire. The time series of the thinning rate from the December 2013 occupation was calculated by comparing the changing phase of the return from the base of the ice shelf with the phase of the internal reflectors. Each averaged burst of 10 chirps was compared with the average from three bursts later, giving temporal averaging of 90 min. The (assumed constant in time and depth) vertical strain rate of the ice column was calculated from two attended profiles at the same site with 1 year separation and used to offset the thinning time series to yield the basal melt rates shown in Figure 5a. The vertical strain-rate contribution to the mean rate of change in range to the base was relatively low (10%).

The most notable characteristic of the time series is the melt rate's variability, ranging up to $6 \, \mathrm{m \, a^{-1}}$ with a mean value for this December time series of $1.6 \, \mathrm{m \, a^{-1}}$. The melt rate at the base of an ice shelf is a function of the

temperature above in situ freezing of the water near the ice base and the water's free stream speed, although other factors (e.g. ice basal roughness and stratification in the water column) also play a role in modulating heat and salt transfer from water to ice. The daily cycle visible in the record, which strongly hints at a tidal influence, should therefore come as no surprise.

The lower panels in Figure 5 show the water temperature (Fig. 5b) and speed (Fig. 5c) measured by an instrument moored 14–15 m below the ice and demonstrate the strong variability that is reflected in the melt rates (e.g. Arzeno and others, 2014). With an average melt rate of $1.6 \, \mathrm{m \, a^{-1}}$, the vertical temperature gradient in the lower part of the ice shelf will be high (e.g. Gade, 1979), so any period of lower water temperature would raise the possibility of enough heat being removed by conduction into the ice base to cause freezing at the interface. A period in which the water temperature was close to, and possibly below, the in situ freezing point was experienced on 12 December 2013, and the ApRES record does indeed show a period of freezing that lasted for 14 hours, peaked at $0.45 \, \mathrm{m \, a^{-1}}$ and resulted in 0.44 mm of ice being deposited.

Vertical profiles of temperature and salinity that were obtained when the borehole was originally drilled showed the possibility of strong temperature gradients in the boundary layer adjacent to the ice base, above the depth of the instruments, probably accounting for the occasional absence of correlation between the measured melt rate and what would be expected from the recorded water temperature and currents. However, the record demonstrates the potential for the technique to be used to improve our understanding of processes that drive heat and salt to the base of the ice shelf, especially when combined with direct measurements of the ocean conditions.
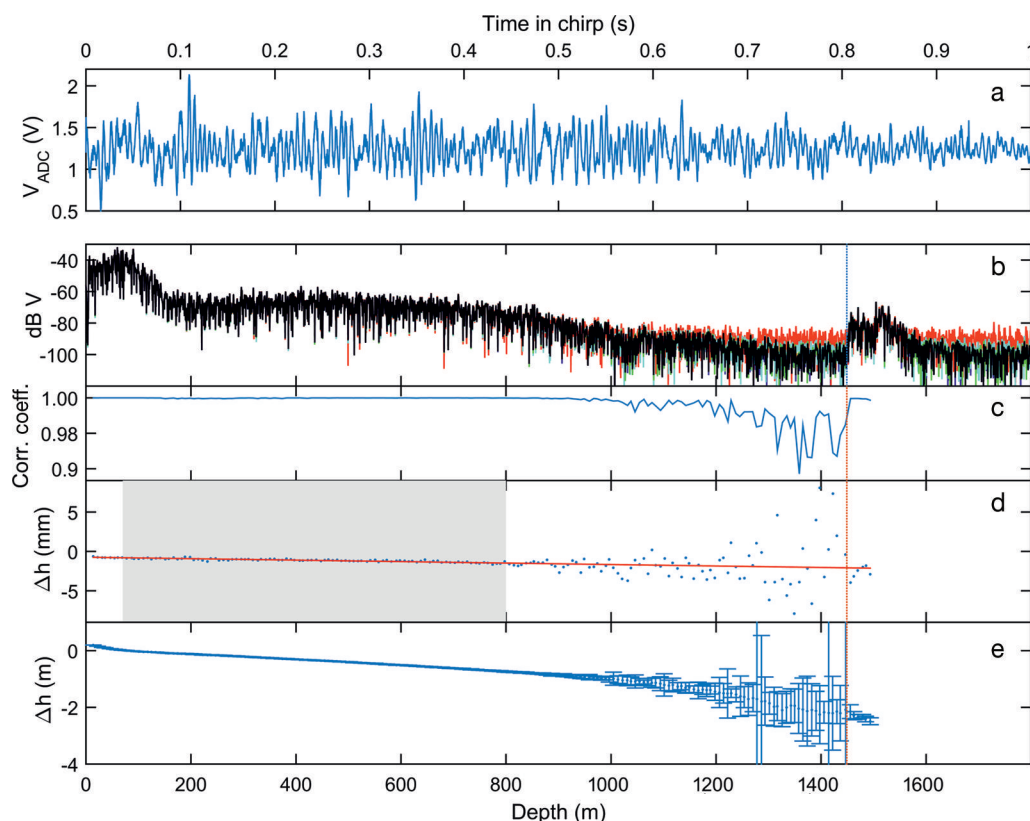
Fig. 6. (a) Raw voltages collected over the 1 s chirp. (b) Fourier transforms of the averages of 1, 10, 100, 500 and 1000 chirps. (c) Amplitude of the correlation coefficient, calculated from overlapping 8 m intervals, between the means of the first and last 500 chirps (time interval of 8 hours). (d) Relative motion of individual 8 m sections over the 8 hour period. Red line is linear fit to section outlined in grey. (e) Same as (d) but over 337 day interval. Note the different vertical scales. Vertical dashed line in (b–e) indicates approximate depth of base.

Pine Island Glacier

Between December 2013 and January 2014 an ApRES system was tested on grounded ice over depths ranging from 1600 to 2400 m, in the catchment of Pine Island Glacier, Antarctica. This study was part of the iStar programme, investigating the ocean forcing on Amundsen Sea ice shelves and the glaciological response. At each of nine sites, the system was left recording for periods of between 8.2 and 30.1 hours. Six of the sites were reoccupied during the 2014/15 field season to obtain the vertical strain within the ice. To demonstrate the radar's performance we present results for one of the sites from the first visit, and briefly show the comparison with the second visit. The aim was to determine the degree of correlation between returns from deep internal layers on consecutive chirps, essential for the calculation of vertical strain rates.

Results from one of the sites, iStar17, are presented in Figure 6. Figure 6a shows the average of 1000, 1 s long, chirps. Unlike the Ross Ice Shelf case, the raw signal is dominated by near-surface returns, giving predominantly lower-frequency contributions. Figure 6b shows 'range domain' versions from Fourier-transforming the averaged data for various ensemble sizes from a single chirp to an average of $N = 1000$. For the system in use at that time the useful limit of averaging was ~500 chirps. In part, that limit appears to be set by the non-ideal nature of the dis-cretization process in signal generation, and in the analogue-to-digital conversion process in signal acquisition, resulting in low-level coherent, system-generated noise that appears after a few hundred averages. With no input to the receiver many tens of thousands of 'chirps' (although no signal is present) can be averaged, with the noise floor still reducing, demonstrating that the receiver itself has relatively low coherent system noise. An additional contribution is from apparently long-range artefacts generated as a result of high-amplitude near-surface returns. These effects are under investigation. Nevertheless, the ApRES signal-to-noise ratio is a substantial improvement on the original vector network analyser-based pRES.

Different techniques are available for measuring how far an internal reflection shifts vertically between remeasurements. One way is to identify peaks in the amplitude of the plot (e.g. Fig. 4b, calculated by Fourier-transforming the chirp) and measure the change in their phase. Another method, used here, is to divide the complex spectrums from each visit into sections (i.e. depth sections) and calculate the cross-correlation between each section from the first visit and the complex conjugate of the corresponding section of the spectrum from the revisit. The phase of each cross-correlation is a direct measure of the relative motion of internal layers within the depth section. The amplitude of the cross-correlation is an indication of how well the internal reflections match between the visits. Figure 6c shows the amplitude of the complex cross-correlation between an average of the first 500 chirps recorded at iStar17 and the last 500 chirps, recorded 8 hours later. Correlations were calculated over a sliding depth window 8 m in width. Values of correlations are high to ~1000 m depth, and thereafter they begin to fall. Varying the width of the depth window has little effect on the depth for which the correlation deteriorates, a depth that appears to be related to a break in slope in the amplitude of the signal (Fig. 6b). Our
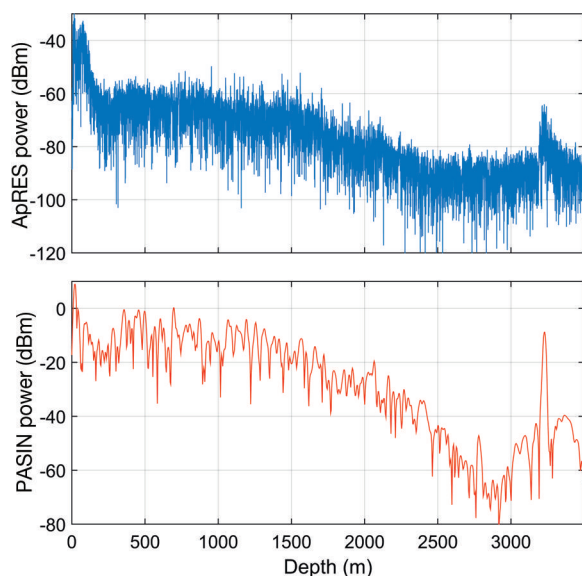
Fig. 7. (a) ApRES return at site near Dome C, using full 200 MHz bandwidth. (b) PASIN return from same location. PASIN's bandwidth is 12 MHz.

working hypothesis is that the signal-to-noise ratio of internal reflections from below 1000 m is too low to allow a stronger correlation. The correlations from the basal returns are high.

An order-of-magnitude estimate for the expected size of vertical strain rate is given by the accumulation rate divided by the ice thickness, or $10^0/10^3 \, a^{-1}$, or $O(10^{-3}) \, a^{-1}$. Over a period of 8 hours, and for the upper kilometre, we would expect differential layer motion of the order of 1 mm. Figure 6d shows the relative motion of internal layers calculated during the 8 hour period of occupation at iStar17. Assuming, for the purposes of this analysis, that the vertical strain rate at this site is constant over the depth interval from 70 m (to exclude compaction in the firn) to 800 m, we fit a straight line through the points, weighting each point by an error estimated from its signal-to-noise ratio, yielding a vertical strain rate of $(-8.5 \pm 0.5) \times 10^{-4} \, a^{-1}$. The quoted error was based on the quality of fit of the regression.

As planned, the iStar sites were revisited during the 2014/15 field season, 11 months after the first occupation. After aligning the depth records to account for surface accumulation between the two visits, the results confirm that the internal layers at iStar17 could be tracked to within one or two hundred metres of the bed at 1450 m, with layers to ~1000 m being closely tracked. Uncertainty in tracking grows over the deepest 30% of the ice column (Fig. 6e). Fitting a straight line to the 70–800 m depth interval gives a vertical strain rate of $(-11.2 \pm 0.06) \times 10^{-4} \, a^{-1}$. It seems, therefore, that even a very short occupation can provide an initial first estimate of the vertical strain rate, given moderate accumulation rates. Other iStar sites had similar depth limits for the correlation, although at one site the correlation was lost at 600 m.

Dome C

During the 2013/14 austral summer, ApRES instruments were taken to Dome C, Antarctica, to attempt to determine the limits of the ability of the radar to monitor the motion of very deep internal layers and therefore contribute to the determination of the ice column's age–depth relationship. There, the

instruments were operated with the skeleton slot antennas, to temperatures of –50°C. To achieve optimum receiver sensitivity the flexibility of direct digital synthesis was utilized. The standard arrangement is designed so that the peak in the range-dependent amplification is for returns from ~2.1 km depth, before slowly rolling off at greater ranges. This feature betrays the original aim of the equipment, which led to it being optimized for use on ice shelves. For the Dome C study, where ice depths are ~3.4 km, the configuration of the instrument was modified so that the chirp lasted for 1.5 s, rather than the usual 1 s. This decreased the FM chirp slope by 67%, causing the 5 kHz amplification peak to correspond to an ice thickness of 3.2 km. Figure 7a demonstrates the effective system performance of the ApRES system by showing a received echo from the ice base with ~35 dB signal-to-noise ratio. Indeed it is probable that with a typical dielectric absorption for ice of 20 dB km^{-1} (two-way) and advantageous basal conditions (a specular ice–water interface) the system would be capable of sounding through our planet's thickest recorded ice (4776 m). For comparison, the echo from the same location that was obtained using the British Antarctic Survey's high-power airborne RES system (Polarimetric Airborne Survey INstrument (PASIN)) is shown in Figure 7b. The fine detail visible in the ApRES return results from its 200 MHz bandwidth, compared with the 12 MHz of the PASIN system. Even though the ApRES transmit power is 0.1 W (compared with the 4 kW of the airborne instrument, a difference of 46 dB) a strong echo is obtained from the coherent stacking of 1000 consecutive radar returns, each of which is of a much longer duration. This coherence demonstrates the stability of the instrument and permits the use of the basal reflector as a reference layer. In this case, absolute vertical velocities can be retrieved as opposed to the relative values obtained using an internal horizon. To ensure that the same ApRES instrument can be used over the next decade to track the movement of the layers throughout the complete ice column, the unit's internal master oscillator was replaced by a GPS-disciplined clock, which has a stability of 1 part in 10^{12} over time intervals measured in years. This effectively removes effects of oscillator ageing and oscillator temperature dependence, necessary for the long-term measurements anticipated for this site.

SUMMARY AND CONCLUSIONS

We have described a phase-coherent ice-sounding radar designed for ground-based surveys either in attended or unattended mode. Conceptually, the instrument is equivalent to the pRES system described by Corr and others (2002), except that the present system uses FMCW, rather than stepped frequency. This new variant is more sensitive, robust, compact and affordable (around US$10k). Unattended, the instrument will run for periods of a year or more (4 year long datasets have now been acquired), collecting several measurements per day with modest power requirements. Unattended operation is designed for environments where the key parameters are varying on timescales from seasonal down to a day or shorter, such as the melt rate at an ice-shelf base. Attended operation is suited to applications where long-term average measurements are acceptable, and where one instrument is to be used to establish many sites, to be revisited at a future time. This is the mode in which pRES is traditionally used, where the sites are typically revisited a year later.

Other than cost, weight, power requirements and ease of use, for attended mode operation the principal advantage of ApRES over pRES is the improved signal-to-noise ratio, allowing internal reflectors to be monitored to depths in excess of 1 km (Pine Island Glacier), and over 2 km at Dome C. The field deployments have demonstrated the system's robustness, stability and system performance. The instrument's performance is superior to that required for our primary aim, which was to provide year-long time series of ice-shelf basal melt rates.

Echoes emanating from reflecting horizons deep within the ice sheet are very weak, and to track their movement requires a high signal-to-noise ratio. We have found that the limit to the depth that the layer motion can be measured is determined by artefacts generated by the transmitter, although possible harmonic contamination from the acquisition system is likely to contribute at some level. The challenge is now to optimize the system to extend the glaciological applications of the instrument.

REFERENCES

Arzeno IB and 7 others (2014) Ocean variability contributing to basal melt rate near the ice front of Ross Ice Shelf, Antarctica. *J. Geophys. Res.*, **119**(7), 4214–4233 (doi: 10.1002/2014jc009792)

Bishop JF and Walton JLW (1981) Bottom melting under George VI Ice Shelf, Antarctica. *J. Glaciol.*, **27**(97), 429–447

Brennan PV, Lok L-B, Nicholls, KW and Corr HFJ (2013) Phase-sensitive FMCW radar system for high-precision Antarctic ice shelf profile monitoring. *IET Radar Sonar Navig.*, **8**(7), 776–786 (doi: 10.1049/iet-rsn.2013.0053)

Corr HFJ, Jenkins A, Nicholls KW and Doake CSM (2002) Precise measurement of changes in ice-shelf thickness by phase-sensitive radar to determine basal melt rates. *Geophys. Res. Lett.*, **29**(8) (doi: 10.1029/2001GL014618)

Dutrieux P and 6 others (2013) Pine Island Glacier ice shelf melt distributed at kilometre scales. *Cryosphere*, **7**(5), 1543–1555 (doi: 10.5194/tc-7-1543-2013)

Dutrieux P and 6 others (2014) Basal terraces on melting ice shelves. *Geophys. Res. Lett.*, **41**(15), 5506–5513 (doi: 10.1002/2014gl060618)

Fricker HA, Hyland G, Coleman R and Young NW (2000) Digital elevation models for the Lambert Glacier–Amery Ice Shelf system, East Antarctica, from ERS-1 satellite radar altimetry. *J. Glaciol.*, **46**(155), 553–560

Gade HG (1979) Melting of ice in sea water: a primitive model with application to the Antarctic ice shelf and icebergs. *J. Phys. Oceanogr.*, **9**(1), 189–198

Gillet-Chaulet F, Hindmarsh RCA, Corr HFJ, King EC and Jenkins A (2011) In-situ quantification of ice rheology and direct measurement of the Raymond Effect at Summit, Greenland using a phase-sensitive radar. *Geophys. Res. Lett.*, **38**, L24503 (doi: 10.1029/2011gl049843)

Jenkins A and Doake CSM (1991) Ice–ocean interactions on Ronne Ice Shelf, Antarctica. *J. Geophys. Res.*, **96**(C1), 791–813 (doi: 10.1029/90jc01952)

Jenkins A, Corr HFJ, Nicholls KW, Stewart CL and Doake CSM (2006) Interactions between ice and ocean observed with phase-sensitive radar near an Antarctica ice-shelf grounding line. *J. Glaciol.*, **52**(178), 325–346 (doi: 10.3189/172756506781828502)

Jenkins A and 6 others (2010) Observations beneath Pine Island Glacier in West Antarctica and implications for its retreat. *Nature Geosci.*, **3**(7), 468–472 (doi: 10.1038/ngeo890)

Kingslake J and 9 others (2014) Full-depth englacial vertical ice sheet velocities measured using phase-sensitive radar. *J. Geophys. Res.*, **119**, 2604–2618 (doi: 10.1002/2014JF003275)

Martin C, Mulvaney R, Gudmundsson GH and Corr HFJ (2015) Inferring palaeo-accumulation records from ice-core data by an adjoint-based method: application to James Ross Island's ice core. *Climate Past*, **11**, 547–557 (doi: 10.5194/cp-11-547-2015)

Moholdt G, Padman L and Fricker HA (2014) Basal mass budget of Ross and Filchner–Ronne ice shelves, Antarctica, derived from Lagrangian analysis of ICESat altimetry. *J. Geophys. Res.*, **119**(11), 2361–2380 (doi: 10.1002/2014jf003171)

Nicholls KW and 21 others (2006) Measurements beneath an Antarctic ice shelf using an autonomous underwater vehicle. *Geophys. Res. Lett.*, **33**, L08612 (doi: 10.1029/2006GL025998)

Nicholls KW, Abrahamsen EP, Heywood KJ, Stansfield K and Østerhus S (2008) High-latitude oceanography using the Autosub autonomous underwater vehicle. *Limnol. Oceanogr.*, **53**(5 pt 2), 2309–2320

Nicholls KW, Østerhus S, Makinson K, Gammelsrød T and Fahrbach E (2009) Ice–ocean processes over the continental shelf of the southern Weddell Sea, Antarctica: a review. *Rev. Geophys.*, **47**, RG3003 (doi: 10.1029/2007RG000250)

Pritchard HD, Arthern RJ, Vaughan DG and Edwards LA (2009) Extensive dynamic thinning on the margins of the Greenland and Antarctic ice sheets. *Nature*, **461**, 971–975 (doi: 10.1038/nature08471)

Rignot E, Jacobs S, Mouginot J and Scheuchl B (2013) Ice-shelf melting around Antarctica. *Science*, **341**(6143), 266–270 (doi: 10.1126/science.1235798)

Schoof C (2007) Ice sheet grounding line dynamics: steady states, stability, and hysteresis. *J. Geophys. Res.*, **112**, F03s28 (doi: 10.1029/2006jf000664)

Shepherd A, Wingham D and Rignot E (2004) Warm ocean is eroding West Antarctic Ice Sheet. *Geophys. Res. Lett.*, **31**(23), L23402 (doi: 10.1029/2004GL021106)

Vaughan DG and 9 others (1995) Subglacial and seabed topography, ice thickness and water column thickness in the vicinity of Filchner-Ronne-Schelfeis, Antarctica. *Polarforschung*, **64**(2), 75–88

Walford MER and Harper MFL (1981) The detailed study of glacier beds using radio-echo techniques. *Geophys. J. R. Astron. Soc.*, **67**(2), 487–514 (doi: 10.1111/j.1365-246X.1981.tb02762.x)

Williams MJM, Jenkins A and Determann J (1998) Physical controls on ocean circulation beneath ice shelves revealed by numerical models. In Jacobs SS and Weiss R eds *Ocean, ice, and atmosphere: interactions at the Antarctic continental margin*. American Geophysical Union, Washington, DC, 285–299 (doi: 10.1029/AR075p0285)